Inorganic Chemistry

pubs.acs.org/IC Article

Design of a Tris-Heteroleptic Ru(II) Complex with Red-Light Excitation and Remarkably Improved Photobiological Activity

Shuang Li, Jian Zhao,* Xinyi Wang, Gang Xu, Shaohua Gou,* and Qiang Zhao*

Cite This: https://dx.doi.org/10.1021/acs.inorgchem.0c01860 Read Online

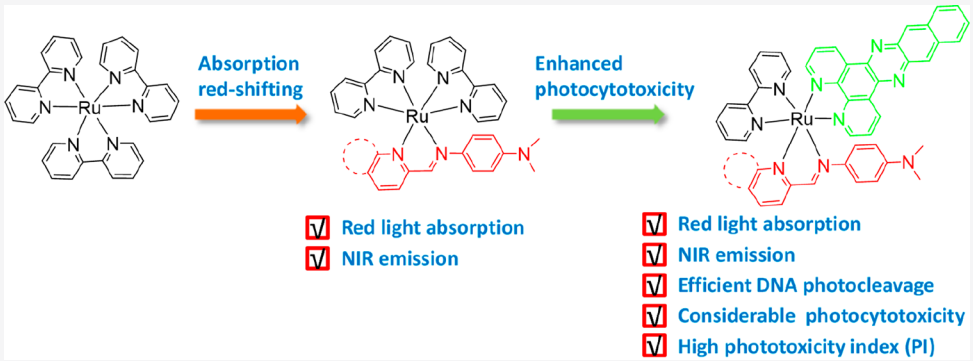

ABSTRACT: Ru(II)-polypyridyl complexes are of increasing interest in photodynamic therapy (PDT) due to their easily tunable photophysical and photochemical properties. However, short-wavelength absorption of Ru(II)-polypyridyl complexes has limited their penetration depth in PDT. Herein, the series of Ru(II)-polypyridyl complexes **1**−**4** was designed by replacing one bipyridine in $[Ru(bpy)_3]Cl_2$ with Schiff bases (iminopyridine or iminoquinoline analogues) to achieve red-shifted absorption of Ru(II)-polypyridyl photosensitizers. To further shift the absorption to longer wavelength and improve the photobiological activity of Ru(II)-polypyridyl complexes, the three tris-heteroleptic Ru(II) complexes **5**−**7** with benzo[*i*]dipyrido[3,2-*a*:2′,3′-*c*]phenazine (dppn) as a ligand were designed to achieve long-lived intraligand (^{3}IL) excited states. Cytotoxicity data against A549 and HepG2 cells revealed that complex **7** showed extraordinarily high cytotoxicity under 650 nm irradiation, resulting in IC_{50} values of 56 and 63 nM with exceptionally large phototoxicity index (PI) values of 763 and 613, respectively. Thus, the resulting complex **7** with considerable red-light photocytotoxicity and high PI values shows a promising potential for therapeutic applications, which represents a new scaffold of Ru(II)-polypyridyl photosensitizers for PDT in the "therapeutic window". This study delivers a rational strategy for the design of tris-heteroleptic Ru(II) complexes as promising photosensitizers for cancer therapy.

■ INTRODUCTION

The successful application of platinum-based anticancer drugs in the clinic has stimulated increasing interest in discovering new metallodrugs, in which ruthenium complexes have been thought to be promising alternatives.[1−6] To date, two ruthenium(III) complexes (NAMI-A, KP1019 and its sodium salt KP1339) have been evaluated in clinical trials for cancer chemotherapy.[7] To further improve the therapeutic efficacy, Ru(II)-polypyridyl complexes with unique photophysical and photochemical properties have been designed as photodynamic therapy (PDT) agents.[8−20] A well-known example is TLD1433, which successfully completed phase Ib clinical trials in 2018.[21]

In PDT, the photosensitizer (PS) used is generally nontoxic in the dark but can be activated to produce cytotoxic reactive oxygen species (ROS) by light of a suitable wavelength.[22−26] As red and near-infrared lights enable maximum tissue penetration with minimum damage, PS activated in the "therapeutic window" of 600−850 nm is suitable for deep-tissue treatment.[27−31] However, the longest-wavelength absorption band (generally a metal to ligand charge transfer (MLCT) transition) of most Ru(II) complexes is located in the blue region (<500 nm), which has limited their phototherapeutic applications for deep-tissue diseases.[32−34] Consequently, exploring novel Ru(II) complexes with one-photon red-light excitation is highly desired for PDT.

Schiff bases are useful for chelating ligands to metal ions, resulting in complexes with different physical and chemical properties.[35] Thus, metal complexes of Schiff bases have been extensively designed and investigated for biomedical applications, such as antitumor, anti-inflammatory, antibacterial, and

Received: June 23, 2020

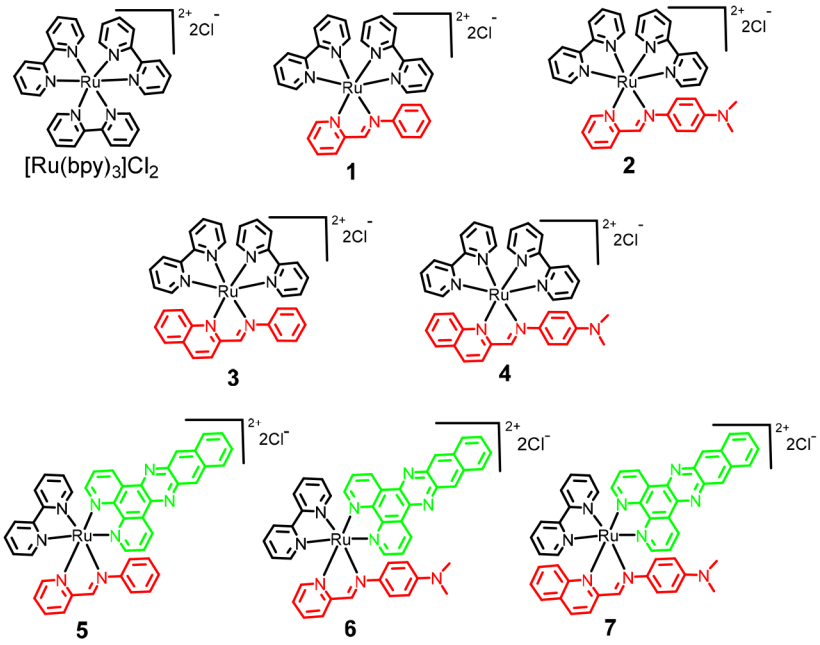

Figure 1. Ru(II)-polypyridyl complexes studied in this work.

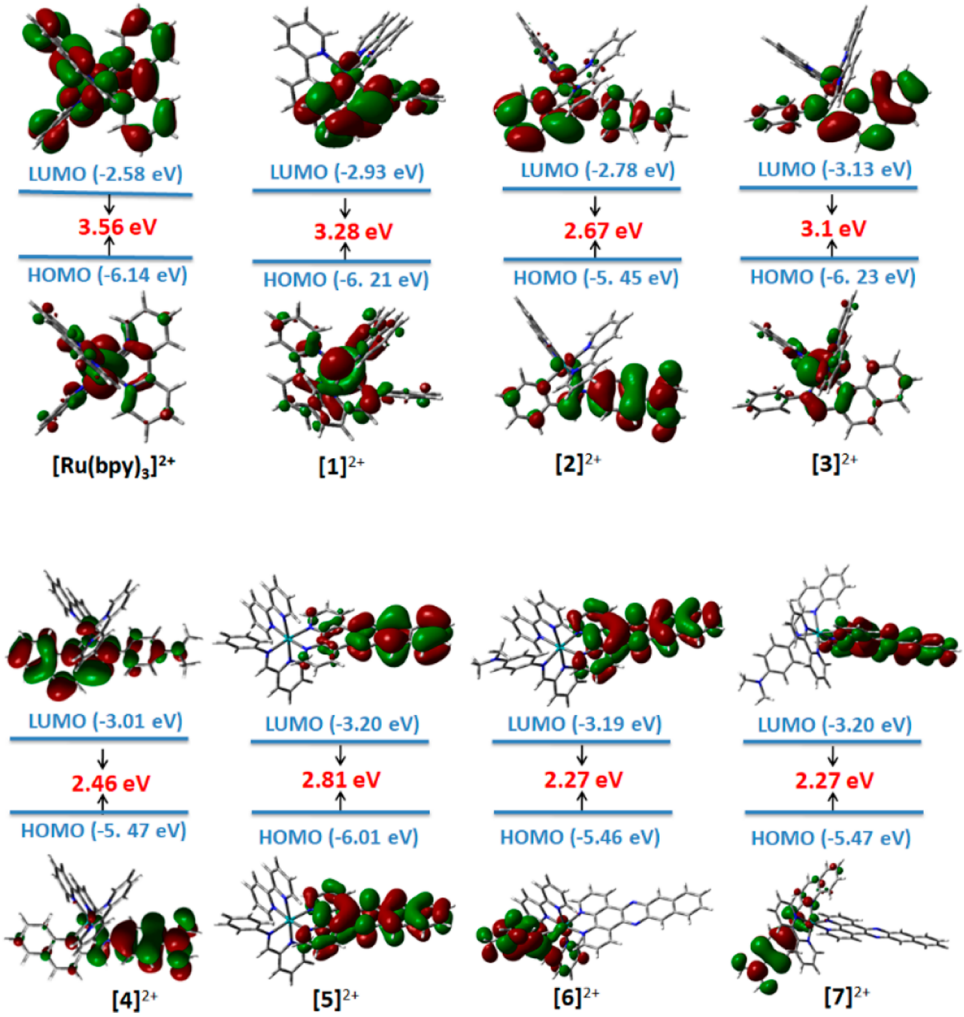

Figure 2. Frontier molecular orbital diagrams and energy profiles for the HOMOs and LUMOs of $[Ru(bpy)_3]^{2+}$ and complexes **1**−**7**.

https://dx.doi.org/10.1021/acs.inorgchem.0c01860
Inorg. Chem. XXXX, XXX, XXX−XXX

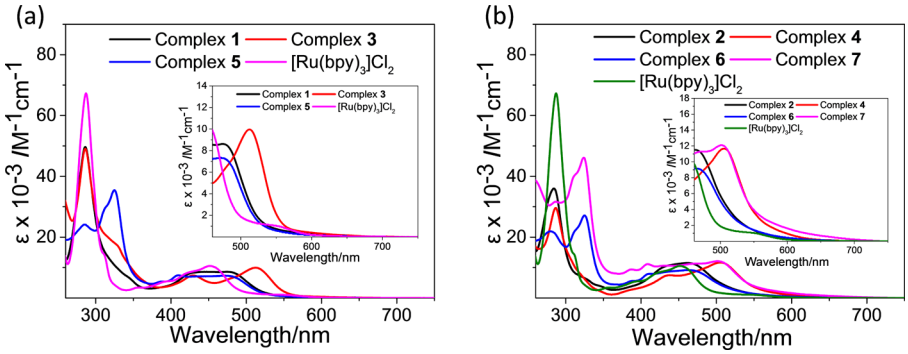

Figure 3. UV−vis absorption spectra of complexes **1**−**7** and $[Ru(bpy)_3]Cl_2$ in methanol. The insets show expansions of the absorption above 460 nm.

antifungal activities.[36] Recently, our group reported that dinuclear Ru(II)-arene complexes containing Schiff base ligands (iminopyridine or iminoquinoline) exhibited unique biological characteristics.[37] Moreover, replacing pyridine ligands with imine ligands in Ru(II) complexes can result in a red shift of the ^{1}MLCT absorption band.[38,39] Therefore, we intend to introduce iminopyridine and iminoquinoline ligands to Ru(II)-polypyridyl complexes with improved photophysical and biological properties for PDT. Herein we utilized $[Ru(bpy)_3]Cl_2$ as a model complex and replaced its one bipyridine with imine ligands to obtain complexes **1**−**4** (Figure 1).

Prior to undertaking the experiments, we performed DFT (density functional theory) calculations to investigate the HOMO/LUMO energy levels of complexes **1**−**4**. As shown in Figure 2, the HOMO−LUMO energy gaps of complexes **1**−**4** are smaller than that of $[Ru(bpy)_3]^{2+}$, which may lead to red shifts of the ^{1}MLCT bands of complexes **1**−**4**, providing a theoretical foundation for the following study.[40] In addition, complexes **2** and **4** possess donor (dimethylamino)−acceptor (pyridine or quinoline) structures, which have relatively lower band gap energies in comparison with complexes **1** and **3**, respectively. However, according to the energy gap law, red-light-absorbing metal complexes often exhibit a short excited-state lifetime that may compromise the therapeutic efficiency of these complexes.[41] Actually, the features of the triplet excited states of metal-based PSs can be tuned for different application purposes such as phototherapy, catalysis, and electroluminescence. Subtle ligand modifications on metal-based PSs can lead to different photophysical and photochemical properties and result in significant changes in the anticancer efficacy.[42] McFarland has demonstrated that Ru(II) complexes with long-lived intraligand (^{3}IL) excited states are extremely sensitive to O_2 and can result in considerable photocytotoxicity.[21,43−46] Moreover, the ^{3}IL excited states of Ru(II)-polypyridyl complexes can be achieved by π-expansive ligands,[21] such as benzo[*i*]dipyrido[3,2-*a*:2′,3′-*c*]phenazine (dppn),[47−49] which can greatly improve the photocytotoxicity of the resulting Ru(II) complexes, as reported by Turro and co-workers.[50] Thus, in order to improve the photobiological activity of Ru(II)-imine complexes, the three tris-heteroleptic Ru(II) complexes **5**−**7** were further designed to achieve long-lived ^{3}IL excited states with dppn as a ligand. It was anticipated that complex **7** with a remarkable red-shifted absorption could exhibit significantly high photocytotoxicity in the PDT therapeutic window.

■ RESULTS AND DISCUSSION

Synthesis and Photophysical Properties. Complexes **1**−**7** were synthesized and characterized as described in the Figures S1−S21 and Scheme S1in the Supporting Information. The UV−vis absorption spectra of these complexes are presented in Figure 3. These complexes exhibit intense absorptions in the ultraviolet region, which are typical absorption bands of Ru(II)-polypyridyl complexes due to the $^1\pi\pi^*$ transitions of the ligands. Notably, the longest absorption maxima of complexes **1**−**7** are located above 470 nm, which are red-shifted in comparison to that of $[Ru(bpy)_3]Cl_2$ at 450 nm. Moreover, complexes **3**, **4**, and **7** with iminoquinoline ligands showed longer wavelength absorption in the visible region in comparison to the corresponding complexes **1**, **2**, and **6** with iminopyridine ligands due to the highly delocalized π-system of the iminoquinoline ligand. In addition, a close examination of the UV−vis absorption spectra of complexes **4** and **7** revealed that the absorption tails of both complexes extend over 650 nm, indicating that they have the potential to be excited by red light. In particular, complex **7** displayed weak but clearly observable absorption bands above 700 nm (700 nm, ε = 200 M^{-1} cm^{-1}). It was reported that Ru(II) complexes with long-lived ^{3}IL excited states are highly sensitive to red-light (630 nm) excitation, which could be excited at wavelengths even where their molar extinction coefficients are very low (ε < 100 M^{-1} cm^{-1}).[21,46] The luminescence spectra of complexes **1**−**7** and $[Ru(bpy)_3]Cl_2$ were studied and are presented in Figure S22. All of the complexes showed near-infrared emission spectra between 700 and 900 nm in methanol, which are red-shifted in comparison to the emission of $[Ru(bpy)_3]Cl_2$, which might be attributed to C═N bond distortion in the excited state.[38] It is noted that the emission intensity of complexes **1**−**7** is so low that the quantum yields are below 1% in deaerated methanol solutions. In addition, the emission of complexes **1**−**7** can be quenched by O_2, demonstrating that the luminescence can be attributed to phosphorescence from the triplet excited state.

Theoretical Calculations. DFT calculations were undertaken to gain insight into the electronic transitions of these Ru(II) complexes, and the fully optimized geometries can be found in Table S1 in the Supporting Information. The selected vertical transition energies between the ground state (S_0) and the singlet excited states (S_n) are presented in Table 1. For complexes **2**, **4**, **6**, and **7**, it is found that the molecular HOMOs are mostly localized on the donor group (dimethylamino), while the LUMOs (LUMO+1 for complexes **6** and **7**) are more localized on the acceptor core (pyridine or

https://dx.doi.org/10.1021/acs.inorgchem.0c01860
Inorg. Chem. XXXX, XXX, XXX−XXX

Table 1. Selected Calculated Singlet Excited-State Transitions for Complexes 1−7 and $[Ru(bpy)_3]Cl_2$

Complex	Trans.	Energy [eV]	f	Major Contribution	Character
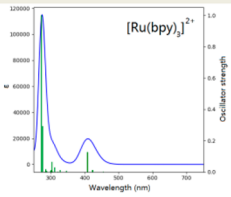	$S_0 \rightarrow S_1$	2.720 (455.9 nm)	0.0003	H → L+1 (78%)	MLCT
	$S_0 \rightarrow S_3$	2.724 (455.1 nm)	0.001	H → L (71%)	MLCT
	$S_0 \rightarrow S_4$	2.903 (427.1 nm)	0.0001	H -1→ L+1 (47%)	MLCT
	$S_0 \rightarrow S_5$	2.926 (423.7 nm)	0.0120	H-1 → L (80%)	MLCT
	$S_0 \rightarrow S_7$	3.034(408.7 nm)	0.1248	H-2 → L (20%)	MLCT
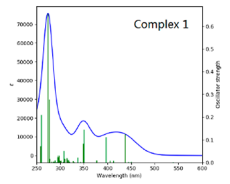	$S_0 \rightarrow S_1$	2.300 (539.1 nm)	0.0012	H → L (96%)	MLCT
	$S_0 \rightarrow S_2$	2.541 (488.0 nm)	0.0002	H-1→ L (95%)	MLCT
	$S_0 \rightarrow S_3$	2.754 (450.2 nm)	0.0026	H → L+1(61%)	MLCT
	$S_0 \rightarrow S_4$	2.787 (444.9 nm)	0.0032	H → L+2 (56%)	MLCT
	$S_0 \rightarrow S_5$	2.831(437.96 nm)	0.1244	H-2 → L (82%)	MLCT
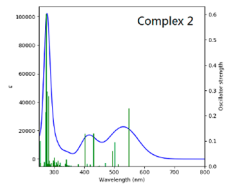	$S_0 \rightarrow S_1$	2.260 (548.7 nm)	0.2288	H → L (76%)	ILCT and MLCT
	$S_0 \rightarrow S_2$	2.415 (513.4 nm)	0.0088	H → L+2 (49%)	LLCT and MLCT
	$S_0 \rightarrow S_3$	2.472 (501.6 nm)	0.0955	H-1→ L (45%)	MLCT
	$S_0 \rightarrow S_4$	2.506 (494.7 nm)	0.0603	H → L+1 (66%)	LLCT and MLCT
	$S_0 \rightarrow S_5$	2.636 (470.1 nm)	0.0134	H-2 → L (80%)	MLCT
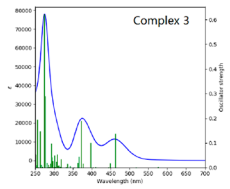	$S_0 \rightarrow S_1$	2.154 (575.7 nm)	0.0027	H → L (94%)	MLCT
	$S_0 \rightarrow S_2$	2.395 (517.6 nm)	0.0008	H-1 → L (61%)	MLCT
	$S_0 \rightarrow S_3$	2.678 (463.1 nm)	0.1374	H-2→ L (52%)	MLCT
	$S_0 \rightarrow S_4$	2.761 (449.0 nm)	0.0186	H → L+2 (88%)	MLCT
	$S_0 \rightarrow S_5$	2.789 (444.5 nm)	0.0009	H → L+1 (96%)	MLCT
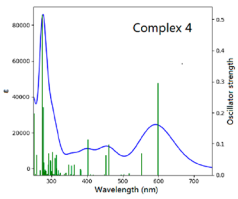	$S_0 \rightarrow S_1$	2.071 (598.8 nm)	0.2958	H → L (86%)	ILCT and MLCT
	$S_0 \rightarrow S_2$	2.241 (553.2 nm)	0.0694	H-1→ L (84%)	MLCT
	$S_0 \rightarrow S_3$	2.396 (517.6 nm)	0.0049	H → L+2 (69%)	LLCT and MLCT
	$S_0 \rightarrow S_4$	2.462 (503.7 nm)	0.0019	H-3→ L(49%)	MLCT
	$S_0 \rightarrow S_5$	2.502 (495.6nm)	0.0006	H → L+1 (67%)	LLCT and MLCT
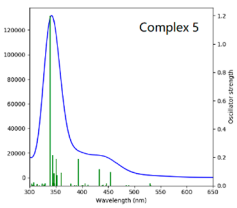	$S_0 \rightarrow S_1$	2.331 (532.0 nm)	0.0013	H-1→ L+1 (94%)	MLCT
	$S_0 \rightarrow S_2$	2.339 (530.1 nm)	0.0169	H → L (98%)	IL
	$S_0 \rightarrow S_3$	2.535 (489.0 nm)	0.0007	H-1 → L (91%)	MLCT
	$S_0 \rightarrow S_4$	2.558 (484.8 nm)	0.0014	H-2→ L+1(94%)	MLCT
	$S_0 \rightarrow S_5$	2.725 (454.9 nm)	0.0934	H-2 → L (89%)	MLCT
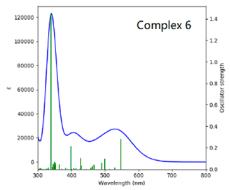	$S_0 \rightarrow S_1$	1.979 (626.7 nm)	0.0007	H → L (99%)	LLCT and MLCT
	$S_0 \rightarrow S_2$	2.267 (547.0 nm)	0.2813	H → L+1 (82%)	ILCT and MLCT
	$S_0 \rightarrow S_3$	2.345 (528.6 nm)	0.0172	H-1 → L (99%)	IL
	$S_0 \rightarrow S_4$	2.416 (513.1 nm)	0.0013	H → L+3 (65%)	LLCT and MLCT
	$S_0 \rightarrow S_5$	2.474 (501.1 nm)	0.0005	H-2 → L (38%)	MLCT
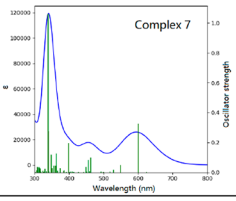	$S_0 \rightarrow S_1$	1.985 (624.5 nm)	0.0021	H → L (99%)	LLCT and MLCT
	$S_0 \rightarrow S_2$	2.068 (599.6 nm)	0.3249	H → L+1(91%)	ILCT and MLCT
	$S_0 \rightarrow S_3$	2.257 (549.4 nm)	0.0499	H-2→ L+1(87%)	MLCT
	$S_0 \rightarrow S_4$	2.342 (529.3 nm)	0.0166	H-1→ L(99%)	IL
	$S_0 \rightarrow S_5$	2.392 (518.3 nm)	0.0043	H → L+3(85%)	LMCT

quinoline). Therefore, the absorption bands (S_0−S_n) of complexes **2**, **4**, **6**, and **7** are composed of ILCT (donor to acceptor) or LLCT (Schiff base ligands to bipyridine/dppn) along with MLCT transitions, while complexes **1**, **3**, and

https://dx.doi.org/10.1021/acs.inorgchem.0c01860
Inorg. Chem. XXXX, XXX, XXX−XXX

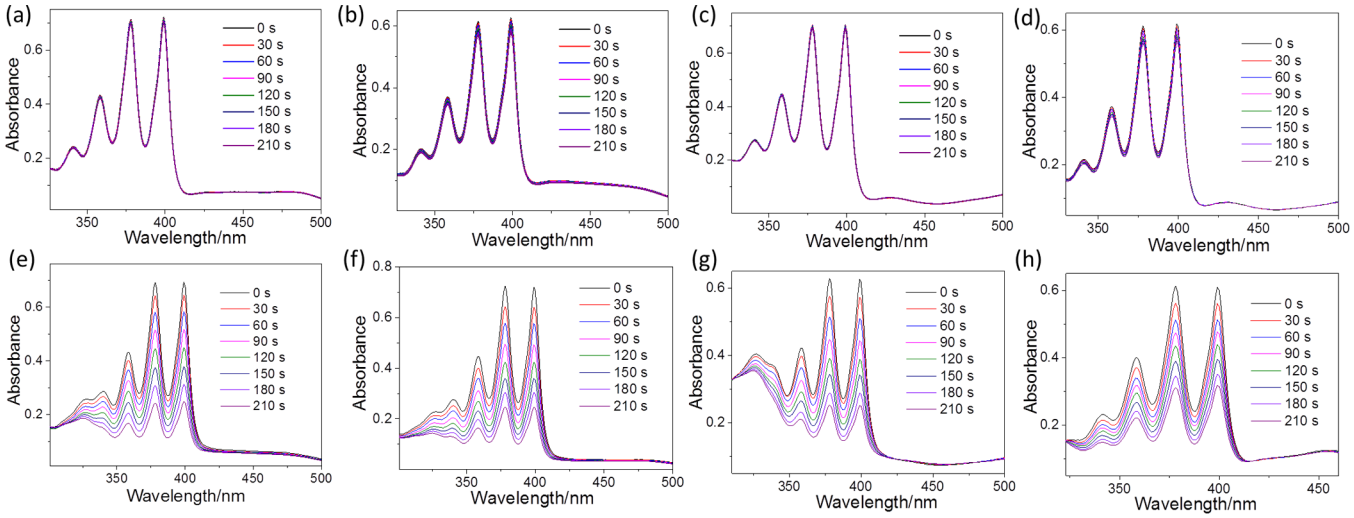

Figure 4. Absorption spectra of ABDA (50 μM) in the presence of **1** (a), **2** (b), **3** (c), **4** (d), **5** (e), **6** (f), **7** (g), and $[Ru(bpy)_3]Cl_2$ (h) at concentrations of 10 μM upon 465 nm irradiation.

Table 2. Photobiological Activity of Complexes 1−7 and $[Ru(bpy)_3]Cl_2$ toward A549 and HepG2 Cancer Cells

	A549					HepG2				
compound	IC_{50}, μM (dark)	IC_{50}, μM (465 nm)	PI[a]	IC_{50}, μM (650 nm)	PI[a]	IC_{50}, μM (dark)	IC_{50}, μM (465 nm)	PI[a]	IC_{50}, μM (650 nm)	PI[a]
1	64.3 ± 2.9	24.9 ± 3.4	2.6	43.8 ± 3.1	1.5	59.4 ± 1.9	23.6 ± 1.7	2.5	40.3 ± 3.1	1.5
2	51.6 ± 3.1	29.5 ± 2.6	1.7	35.5 ± 3.5	1.5	48.5 ± 2.4	25.8 ± 2.3	1.9	37.1 ± 2.2	1.3
3	52.5 ± 2.6	22.6 ± 1.3	2.3	30.4 ± 1.7	1.7	55.7 ± 4.6	34.1 ± 3.1	1.6	33.6 ± 2.5	1.7
4	49.6 ± 3.7	16.2 ± 1.1	3.1	18.8 ± 1.2	2.6	45.9 ± 2.7	11.5 ± 1.0	4.0	17.3 ± 1.4	2.7
5	51.8 ± 3.3	0.089 ± 0.008	582	0.242 ± 0.006	214	46.4 ± 3.0	0.065 ± 0.008	713	0.231 ± 0.012	201
6	48.7 ± 2.8	0.073 ± 0.011	667	0.149 ± 0.005	327	40.4 ± 2.5	0.045 ± 0.006	897	0.132 ± 0.007	306
7	42.7 ± 3.5	0.038 ± 0.003	1124	0.056 ± 0.004	763	38.6 ± 2.1	0.040 ± 0.003	965	0.063 ± 0.004	613
$[Ru(bpy)_3]Cl_2$	54.4 ± 4.7	8.5 ± 0.6	6.4	53.1 ± 1.6	1.0	53.2 ± 4.2	7.5 ± 0.4	7.1	49.1 ± 1.8	1.1

[a]PI = dark IC_{50} value/light IC_{50} value.

$[Ru(bpy)_3]^{2+}$ are composed of MLCT transitions (Table 1 and Figures S23−S30). In addition, the calculated energy level of the S_1 state of $[Ru(bpy)_3]^{2+}$ is 2.72 eV (456 nm), which is higher than those of complexes **1**−**7**, in accordance with the experimental results that the absorption tails of complexes **1**−**7** terminate at longer wavelength in comparison with $[Ru(bpy)_3]^{2+}$.

$^1O_2$ Generation. The singlet oxygen ($^1O_2$) generation ability was evaluated for complexes **1**−**7** together with $[Ru(bpy)_3]Cl_2$ as a control by using 9,10-anthracenediyl-bis(methylene)dimalonic acid (ABDA) as a probe, which can react with $^1O_2$ and convert to a steady-state endoperoxide product, thereby leading to a decrease in absorption intensity at around 378 nm. As shown in Figure 4, the absorbance of ABDA decreased dramatically in the presence of complexes **5**−**7** and $[Ru(bpy)_3]Cl_2$ upon 465 nm irradiation (1.26 J cm^{-2}), whereas a slight decrease in ABDA absorbance was observed for complexes **1**−**4**. By using $[Ru(bpy)_3]Cl_2$ as a reference (Φ_Δ = 0.41 in water),[51] the $^1O_2$ quantum yields of complexes **1**−**7** were determined to be 0.025, 0.036, 0.061, 0.046, 0.27, 0.33, and 0.36, respectively, revealing that complexes **5**−**7** and $[Ru(bpy)_3]Cl_2$ are capable of producing $^1O_2$ more efficiently than complexes **1**−**4** under 465 nm irradiation.

Considering the red-light absorption ability of complexes **1**−**7**, we further investigated their $^1O_2$ generation with irradiation at 650 nm (19.2 J cm^{-2}) (Figure S31). As expected, complexes **4** and **7** can lead to an obvious decrease in ABDA absorbance, indicating that they are capable of producing $^1O_2$ under 650 nm light irradiation. Strikingly, complexes **5** and **6** with low molar absorption coefficients at 650 nm can cause severe reduction in ABDA, which is probably due to their highly photosensitizing ^{3}IL excited states.[45] In addition, little decrease in ABDA absorbance was observed for complexes **1**−**3** and $[Ru(bpy)_3]Cl_2$ due to their negligible molar absorption coefficients in the red-light region. This study indicates that complexes **4**−**7** could be excited by red light, which provided the conditions for these complexes to realize PDT.

In Vitro Photocytotoxicity. The in vitro photocytotoxicity of complexes **1**−**7** was evaluated against A549 and HepG2 cancer cells by using an MTT assay, together with $[Ru(bpy)_3]Cl_2$ for comparison (Table 2 and Figure S32). Upon blue-light irradiation (465 nm), the photocytotoxicity enhancement of complexes **1**−**4** and $[Ru(bpy)_3]Cl_2$ toward the tested cell lines is modest with PI (phototoxicity index) values ranging from 1.6 to 7.1 (Table 2). Unexpectedly, complexes **5**−**7** exhibited greatly enhanced cytotoxicity against A549 and HepG2 cancer cells with blue-light irradiation, resulting in IC_{50} values ranging from 38 and 89 nM with exceptionally large PI values from 582 to 1124, respectively, which are 2 orders of magnitude larger than those of complexes **1**−**4**. This may be attributed to the highly photosensitizing ^{3}IL excited state of complexes **5**−**7**. Importantly, upon red-light irradiation (650

https://dx.doi.org/10.1021/acs.inorgchem.0c01860
Inorg. Chem. XXXX, XXX, XXX−XXX

nm), considerable cytotoxicity was also observed for complexes **5**−**7** against A549 and HepG2 cells with PI values ranging from 201 to 763. In contrast, complexes **1**−**4** and $[Ru(bpy)_3]Cl_2$ produced no discernible photodynamic activities (PI = 1.0−2.7) upon irradiation with red light. When these results are taken together, complex **7** with the most considerable red-light photocytotoxicity as well as the highest PI value within these complexes shows a promising potential for therapeutic applications.

To further confirm the considerable photocytotoxicity of complex **7**, a calcein AM and propidium iodide (PI) costaining assay was carried out to label the living and dead cells as indicators by staining the cytoplasm with the green fluorescence generated by the enzymatic hydrolysis of calcein AM and the nucleus with the red fluorescence of PI, respectively (Figure 5 and Figure S33). In addition, complex

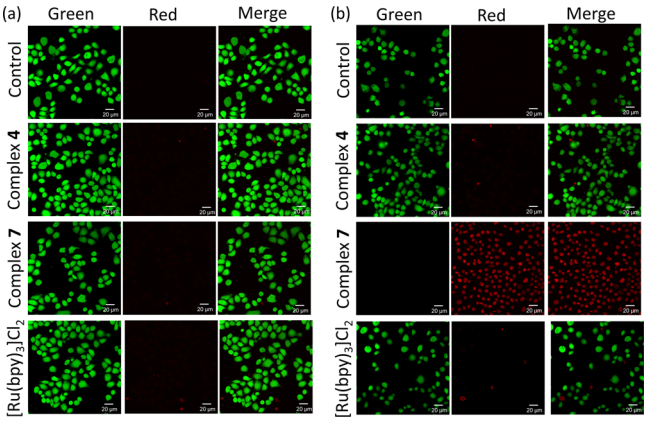

Figure 5. Confocal fluorescence images of calcein AM (green, live cells)/propidium iodide (PI; red, dead cells) costained A549 cells after treatment with complexes **4**, **7**, and $[Ru(bpy)_3]Cl_2$ at concentrations of 1 μM: (a, left) without irradiation, (b, right) irradiation at 650 nm.

4 and $[Ru(bpy)_3]Cl_2$ were also studied for comparison. As shown in Figure 5a, no significant cell death was observed without irradiation for A549 cells after treatment with complexes **4**, **7** and $[Ru(bpy)_3]Cl_2$. Once irradiation was conducted under 465 or 650 nm, cells treated by complex **7** were effectively killed as revealed by the intense red fluorescence, whereas complex **4** or $[Ru(bpy)_3]Cl_2$ treated cells were negligibly damaged, demonstrating the robust PDT ability of complex **7** again.

Intracellular ROS Production. The intracellular ROS generation in A549 cells after treated with complexes **4**, **7**, and $[Ru(bpy)_3]Cl_2$ was evaluated using a 2,7-dichlorodihydrofluorescein diacetate (DCFH-DA) staining method. DCFH-DA is a nonfluorescent cell-permeable indicator for ROS, which can be converted to the highly fluorescent DCF upon intracellular oxidation by ROS. As shown in Figure 6, no ROS production was observed in A549 cells without light irradiation. However, after they were exposed to 465 nm light irradiation, the compound-treated A549 cells showed obvious green fluorescence, demonstrating the successful production of ROS. Notably, in the presence of 650 nm illumination, ROS production was detected after the cells were treated with complexes **4** and **7**. In contrast, negligible ROS signals were observed in $[Ru(bpy)_3]Cl_2$-treated cells, matching well with the extracellular $^1O_2$ generation results.

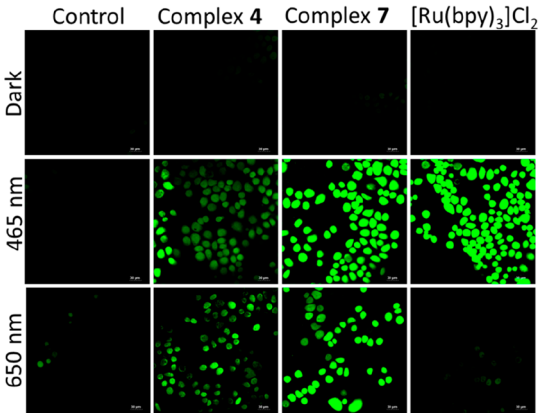

Figure 6. Confocal fluorescence images of ROS generation in A549 cells incubated with complexes **4** and **7** and $[Ru(bpy)_3]Cl_2$ upon 465 and 650 nm irradiation.

Cellular Accumulation. To investigate the possible mechanism of the considerable photocytotoxicity of complex **7** on A549 cancer cells, the intracellular content of Ru was detected using ICP-MS (inductively coupled plasma mass spectrometry) together with complex **4** and $[Ru(bpy)_3]Cl_2$ for comparison. As shown in Figure S34, there was no obvious difference of the intracellular Ru contents for complex **4** (91.7 ± 8.3 ng/10^5 cells) and **7** (98 ± 7.2 ng/10^5 cells). Thus, it is rational to conclude that the cellular accumulation is not the main reason for the markedly improved photocytotoxicity of complex **7**.

DNA Photocleavage. Ru(II)-polypyridyl complexes are known to induce DNA photocleavage, which may be responsible for the observed photocytotoxicity to some extent. Thus, the DNA photocleavage ability of complex **7** was investigated under blue (465 nm)- and red-light (650 nm) irradiation by agarose gel electrophoresis together with complex **4** and $[Ru(bpy)_3]Cl_2$ for comparison. As shown in Figure 7A, complex **4** did not show any observable DNA

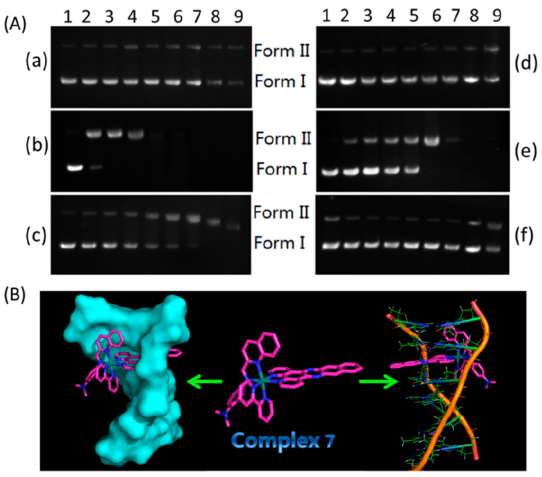

Figure 7. (A) Gel electrophoretic mobility pattern of pBR322 plasmid DNA incubated with various concentrations of Ru(II) complexes under blue and/or red light irradiation. Lanes 1−9 (0, 1, 5, 20, 40, 80, 160, 320, and 640 μM) + DNA: (a) **4** + 465 nm; (b) **7** + 465 nm; (c) $[Ru(bpy)_3]Cl_2$ + 465 nm; (d) **4** + 650 nm; (e) **7** + 650 nm; (f) $[Ru(bpy)_3]Cl_2$ + 650 nm. (B) Stereoview of the molecular docking of complex **7** with DNA duplex (PDB ID: 4JD8).

https://dx.doi.org/10.1021/acs.inorgchem.0c01860
Inorg. Chem. XXXX, XXX, XXX−XXX

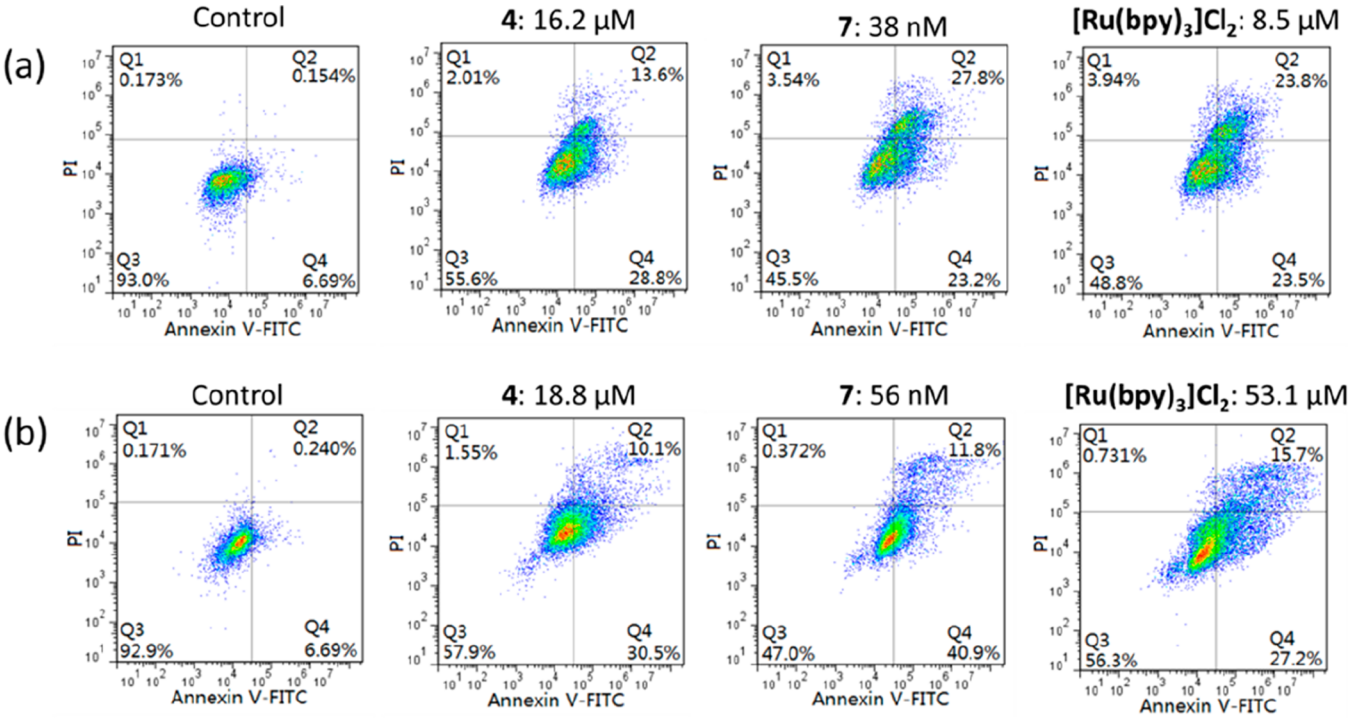

Figure 8. Flow cytometry analysis for apoptosis of A549 cancer cells in the presence of (a) blue light and (b) red light.

cleavage at the tested concentrations under blue light irradiation. In contrast, complex **7** exhibited considerable DNA photocleavage activity, which can completely convert supercoiled DNA form (form I) to nicked circular form (form II) at an extremely low concentration of 5 μM (drug to nucleotide ratio: 0.032). Moreover, the plasmid DNA gradually disappeared with increasing concentrations of complex **7**, indicating that it can inhibit the intercalation of EtBr in plasmid DNA at high concentrations. In addition, $[Ru(bpy)_3]Cl_2$ displayed much weaker DNA photocleavage activity in comparison to complex **7** under the experimental conditions. For the red-light irradiation, a concentration-dependent DNA cleavage pattern was also observed for complex **7**, while complex **4** and $[Ru(bpy)_3]Cl_2$ did not show any obvious cleavage, which is indicative of the efficient DNA photocleavage ability of complex **7** upon red-light irradiation. When these results are taken together, the considerable DNA photocleavage activity of complex **7** may be one of the causes for its high photocytotoxicity.

The binding of the PS to DNA is a key step for DNA photocleavage.[52] It has been reported that dppz-containing Ru(II) complexes (dppz = dipyrido[3,2-*a*:2′,3′-*c*]phenazine) can intercalate between DNA base pairs and serve as DNA molecular light switches.[53] The dppn ligand in complex **7** is a derivative of dppz, which may have the potential to intercalate into DNA due to the excellent planar conjugated structure of dppn.[54,55] Thus, a molecular docking study was carried out on a DNA duplex structure (PDB ID: 4JD8) to elucidate the DNA binding mode of complex **7** using the AutoDock 4.2 package.[56,57] Obviously, complex **7** showed an intercalation behavior similar to that of dppz-containing Ru(II) complexes (Figure 7B), and the binding energy was calculated to be −10.78 kcal/mol, indicating that complex **7** can effectively bind to the DNA. When these results are taken together, the considerable DNA photocleavage activity of complex **7** may be ascribed to its strong DNA binding ability as well as high $^1O_2$ generation efficiency.

Cell Death Study. The potential of complexes **4** and **7** and $[Ru(bpy)_3]Cl_2$ to induce cell death was determined with blue (465 nm)- and red-light (650 nm) irradiation by using an Annexin V-FITC/propidium iodide (PI) assay. A549 cancer cells were treated with the Ru(II) complexes at concentrations of their IC_{50} values. As shown in Figure 8, all Ru(II) complexes can induce obvious incidences of early- to late-stage apoptosis in A549 cancer cells in comparison with untreated cells (control) under blue- and red-light irradiation with apoptotic rates of ∼50%. This result was in accordance with the results of the MTT assay. Overall, this study indicates that the two Ru(II) complexes produced cancer cell death through an apoptotic pathway under light exposure.

■ CONCLUSION

In summary, complexes **1**−**7** were designed as analogues to $[Ru(bpy)_3]Cl_2$ with the aim to red-shift the ^{1}MLCT absorption of Ru(II)-polypyridyl complexes into the PDT window (600−850 nm). DFT calculations indicated that the HOMO−LUMO energy gaps of complexes **1**−**7** are much smaller than that of $[Ru(bpy)_3]^{2+}$, which is responsible for the red shifting of the ^{1}MLCT absorption band of these complexes. Cytotoxicity data against A549 and HepG2 cells revealed that complex **7** showed extraordinarily high cytotoxicity under 650 nm irradiation, resulting in IC_{50} values of 56 and 63 nM with exceptionally large phototoxicity index (PI) values of 763 and 613, respectively. Thus, the resulting complex **7** with considerable red-light photocytotoxicity and high PI values shows a promising potential for therapeutic applications, which represents a new scaffold of Ru(II)-polypyridyl photosensitizers for PDT in the "therapeutic window". This study delivers a rational strategy for the design of tris-heteroleptic Ru(II) complexes as promising photosensitizers for cancer therapy.

https://dx.doi.org/10.1021/acs.inorgchem.0c01860
Inorg. Chem. XXXX, XXX, XXX−XXX

■ EXPERIMENTAL SECTION

Materials and Measurements. All analytical grade chemicals and solvents were used without further purification. *cis*-[Ru(bpy)(dppn)Cl_2] was prepared according to previous literature methods.[49] ^{1}H and ^{13}C NMR spectra were recorded on a Bruker Avance III-HD 600 MHz spectrometer. Elemental analysis of C, H, and N used a Vario MICRO CHNOS elemental analyzer (Elementar). UV−vis absorption and luminescence spectra were measured on a Shimadzu UV2600 instrument and a FluoroMax-4 fluorometer, respectively. Mass spectrometry was performed using an Agilent 6224 ESI/TOF MS instrument. Cell accumulation was conducted on a PerkinElmer NexION 1000G ICP mass spectrometer.

Preparation of 1. Complex **1** was prepared according to previous literature.[38] Yield: 0.57 g (71.3%), yellowish brown powder. Anal. Calcd for $C_{32}H_{26}Cl_2N_6Ru$: C, 57.66; H, 3.93; N, 12.61. Found: C, 57.71; H, 3.91; N, 12.64. ESI mass spectrum data: *m*/*z* 298.0647 ([M/2 − Cl]$^+$). ^{1}H NMR (600 MHz, DMSO-d_6): δ 6.63 (d, *J* = 7.6 Hz, 2H), 7.07 (t, *J* = 7.8 Hz, 2H), 7.16 (t, *J* = 7.4 Hz, 1H), 7.35 (t, *J* = 6.6 Hz, 1H), 7.53 (t, *J* = 6.2 Hz, 1H), 7.61−7.65 (m, 2H), 7.67−7.73 (m, 3H), 7.75 (d, *J* = 5.4 Hz, 1H), 7.85 (d, *J* = 5.5 Hz, 1H), 7.90 (m, 1H), 8.26−8.28 (m, 4H), 8.44 (d, *J* = 8.1 Hz, 1H), 8.58 (d, *J* = 7.7 Hz, 1H), 8.64 (d, *J* = 8.2 Hz, 1H), 8.69 (d, *J* = 5.3 Hz, 1H), 8.94−9.00(m, 2H), 9.42 (s, 1H). ^{13}C NMR (150 MHz, DMSO-d_6): δ 121.60, 124.06, 124.27, 125.15, 125.23, 127.79, 128.29, 128.55, 128.58, 128.70. 129.33, 129.55, 131.25, 138.02, 138.17, 138.60, 138.68, 138.77, 148.98, 151.64, 151.73, 152.05, 152.18, 153.43, 156.54, 156.76, 156.82, 156.93, 157.31, 169.88.

General Procedure for the Synthesis of Complexes 2−7. A methanol solution (30 mL) of aniline (for the synthesis of complexes **3** and **5**) or *N*,*N*-dimethyl-1,4-phenylenediamine (for the synthesis of complexes **2**, **4**, **6**, and **7**) (1.2 mmol) and the corresponding aldehydes (1.2 mmol) was heated at reflux for 12 h to obtain a yellowish brown solution. The solution was used without purification. Then *cis*-[Ru(bpy)$_2$$Cl_2$] or *cis*-[Ru(bpy)(dppn)Cl_2] (1.0 mmol) was added, and the resulting mixture was stirred under reflux for 12 h, during which time the mixture turned dark brown. The solvent was then removed by evaporation under reduced pressure. The crude product was purified using dichloromethane/methanol (20/1, v/v) through preparative column chromatography (basic Al_2O_3) to afford the product.

Complex 2. Yield: 0.58 g (68.11%), yellowish brown powder. Anal. Calcd for $C_{34}H_{31}Cl_2N_7Ru$: C, 57.55; H, 4.40; N, 13.82. Found: C, 57.58; H, 4.39; N, 13.86. ESI mass spectrum data: *m*/*z* 319.5857 ([M/2 − Cl]$^+$). ^{1}H NMR (600 MHz, DMSO-d_6): δ 2.81 (s, 6H), 6.31 (d, *J* = 9.0 Hz, 2H), 6.59 (d, *J* = 8.6 Hz, 2H), 7.41 (t, *J* = 6.6 Hz, 1H), 7.52−7.58 (m, 2H), 7.64 (d, *J* = 5.0 Hz, 1H), 7.73−7.65 (m, 3H), 7.73−7.77 (m, 2H), 7.96−8.02 (m, 1H), 8.24−8.15 (m, 3H), 8.25 (m, 1H), 8.52−8.63 (m, 3H), 8.74 (t, *J* = 9.3 Hz, 1H), 9.02 (m, 2H), 9.29−9.34 (m, 1H). ^{13}C NMR (150 MHz, DMSO-d_6): δ 48.99, 111.66, 122.95, 124.33, 128.52, 137.97, 138.53, 138.67, 150.56, 151.47, 151.70, 151.73, 151.81, 153.31, 156.75, 156.88, 157.02, 157.82, 165.42.

Complex 3. Yield: 0.45 g (52.33%), reddish brown powder. Anal. Calcd for $C_{36}H_{28}Cl_2N_6Ru$: C, 60.34; H, 3.94; N, 11.73. Found: C, 60.40; H, 3.92; N, 11.75. ESI mass spectrum data: *m*/*z* 323.0726 ([M/2 − Cl]$^+$). ^{1}H NMR (600 MHz, DMSO-d_6): δ 6.59 (d, *J* = 7.3 Hz, 2H), 7.08 (t, *J* = 7.2 Hz, 2H), 7.16 (t, *J* = 7.0 Hz, 1H), 7.24 (d, *J* = 8.9 Hz, 2H), 7.39 (t, *J* = 7.5 Hz, 1H), 7.49 (d, *J* = 4.8 Hz, 1H), 7.61−7.67 (m, 3H), 7.73 (t, *J* = 7.2 Hz, 1H), 7.88 (d, *J* = 12.7 Hz, 2H), 8.00 (d, *J* = 4.8 Hz, 1H), 8.15 (t, *J* = 7.6 Hz, 1H), 8.22 (d, *J* = 7.9 Hz, 1H), 8.24−8.30 (m, 2H), 8.48 (d, *J* = 7.8 Hz, 1H), 8.65 (d, *J* = 7.5 Hz, 2H), 8.77 (d, *J* = 7.8 Hz, 1H), 8.84−8.93 (m, 2H), 8.99 (d, *J* = 7.9 Hz, 1H), 9.83 (s, 1H). ^{13}C NMR (150 MHz, DMSO-d_6): δ 121.37, 124.15, 124.71, 125.05, 125.41, 125.05, 125.41, 125.97, 127.93, 128.34, 128.41, 128.71, 128.80, 129.26, 129.99, 130.04, 130.42, 132.39, 138.42, 138.66, 139.14, 139.21, 139.55, 149.21, 149.66, 151.29, 151.81, 152.33, 153.78, 156.68, 156.84, 157.08, 158.99, 172.53.

Complex 4. Yield: 0.48 g (63.5%), reddish brown powder. Anal. Calcd for $C_{38}H_{33}Cl_2N_7Ru$: C, 60.08; H, 4.38; N, 12.91. Found: C, 60.19; H, 4.35; N, 12.94. ESI mass spectrum data: *m*/*z* 344.5973 ([M/2 − Cl]$^+$). ^{1}H NMR (600 MHz, DMSO-d_6): δ 2.81 (s, 6H), 6.30−6.32 (d, 2H, *J* = 8.9 Hz), 6.50−6.51 (d, 2H, *J* = 8.9 Hz), 7.15−7.16 (d, 1H, *J* = 8.9 Hz), 7.30−7.32 (t, 1H, *J* = 6.6 Hz), 7.34−7.36 (m, 1H), 7.52−7.53 (d, 1H, *J* = 5.4 Hz), 7.58−7.60 (t, 1H, *J* = 5.4 Hz), 7.62−7.65 (q, 2H, *J* = 6.4 Hz), 7.67−7.70 (t, 1H, *J* = 7.5 Hz), 7.80−7.81 (t, 1H, *J* = 5.3 Hz), 7.95−7.97 (t, 1H, *J* = 7.6 Hz), 7.98−7.99 (d, 1H, *J* = 5.4 Hz), 8.15−8.19 (m, 2H), 8.24−8.27 (t, 2H, *J* = 7.8 Hz), 8.54−8.55 (d, 1H, *J* = 5.4 Hz), 8.56−8.60 (d-d, 2H, J_1 = 8.5 Hz, J_2 = 12.4 Hz), 8.79−8.82 (m, 2H), 8.90−8.91 (d, 1H, *J* = 8.2 Hz), 8.99−9.01 (d, 1H, *J* = 8.2 Hz), 9.67 (s, 1H). ^{13}C NMR (150 MHz, DMSO-d_6): δ 40.34, 111.68, 122.65, 123.96, 124.33, 124.66, 125.08, 125.41, 125.52, 127.88, 128.29, 128.62, 128.64, 129.60, 129.75, 130.38, 132.18, 138.39, 138.55, 138.89, 139.10, 139.23, 139.30, 149.73, 150.43, 151.39, 151.58, 152.42, 153.43, 156.77, 156.85, 157.05, 157.21, 159.49, 169.01.

Complex 5. Yield: 0.28 g (33.2%), reddish brown powder. Anal. Calcd for $C_{44}H_{30}Cl_2N_8Ru$: C, 62.71; H, 3.59; N, 13.30. Found: C, 62.73; H, 3.53; N, 13.31. ESI mass spectrum data: *m*/*z* 386.0775 ([M/2 − Cl]$^+$). ^{1}H NMR (600 MHz, DMSO-d_6): δ ^{1}H NMR (600 MHz, DMSO): δ 6.75 (d, *J* = 7.6 Hz, 2H), 7.11 (t, *J* = 7.8 Hz, 2H), 7.25−7.16 (m, 2H), 7.53−7.48 (m, 1H), 7.77−7.73 (m, 4H), 7.83 (d, *J* = 5.2 Hz, 1H), 7.89−7.85 (m, 1H), 7.91 (d, *J* = 5.6 Hz, 1H), 8.02 (dd, *J* = 8.1, 5.4 Hz, 1H), 8.25−8.15 (m, 3H), 8.29 (td, *J* = 8.1, 1.2 Hz, 1H), 8.50−8.41 (m, 3H), 8.62 (d, *J* = 7.8 Hz, 1H), 8.71 (d, *J* = 8.3 Hz, 1H), 9.19 (dd, *J* = 5.2, 0.9 Hz, 1H), 9.23 (d, *J* = 8.7 Hz, 2H), 9.49 (s, 1H), 9.59 (dd, *J* = 8.1, 1.0 Hz, 1H), 9.66 (dd, *J* = 8.1, 1.0 Hz, 1H). ^{13}C NMR (150 MHz, DMSO-d_6): δ 121.78, 123.98, 124.33, 127.60, 128.28, 128.45, 128.62, 128.74, 129.10, 129.39, 131.13, 131.22, 133.82, 133.95, 135.08, 138.06, 138.29, 138.37, 138.96, 141.61, 141.64, 148.99, 151.21, 151.32, 152.44, 152.51, 152.80, 154.00, 155.63, 156.55, 157.20, 169.93.

Complex 6. Yield: 0.35 g (39.5%), reddish brown powder. Anal. Calcd for $C_{46}H_{35}Cl_2N_9Ru$: C, 63.41; H, 4.17; N, 13.91. Found: C, 63.38; H, 4.19; N, 13.94. ESI mass spectrum data: *m*/*z* 407.5984 ([M/2 − Cl]$^+$). ^{1}H NMR (600 MHz, DMSO-d_6): δ 2.35 (s, 6H), 6.01 (d, *J* = 9.1 Hz, 2H), 6.43 (d, *J* = 9.0 Hz, 2H), 7.47 (t, *J* = 6.4 Hz, 1H), 7.67−7.62 (m, 1H), 7.72−7.67 (m, 2H), 7.80−7.76 (m, 1H), 7.87 (t, *J* = 6.2 Hz, 2H), 7.95 (d, *J* = 5.4 Hz, 1H), 8.14−8.13 (m, 1H), 8.16 (dd, *J* = 8.0, 5.3 Hz, 1H), 8.21−8.18 (m, 2H), 8.26−8.22 (m, 1H), 8.32 (dd, *J* = 11.7, 4.4 Hz, 1H), 8.38−8.35 (m, 2H), 8.59 (d, *J* = 7.8 Hz, 1H), 8.69 (d, *J* = 5.2 Hz, 1H), 9.04 (d, *J* = 11.1 Hz, 2H), 9.10−9.06 (m, 2H), 9.33−9.31 (m, 1H), 9.35 (s, 1H), 9.54 (dd, *J* = 8.0, 1.1 Hz, 1H). ^{13}C NMR (150 MHz, DMSO-d_6): δ 40.55, 111.59, 122.82, 128.29, 128.44, 129.06, 130.09, 130.15, 135.02, 138.09, 138.21, 138.73, 140.84, 150.08, 150.90, 151.11, 156.90, 157.09, 157.98, 166.10.

Complex 7. Yield: 0.22 g (24.0%), reddish brown powder. Anal. Calcd for $C_{50}H_{37}Cl_2N_9Ru$: C, 64.17; H, 3.99; N, 13.47. Found: C, 64.22; H, 4.02; N, 13.49. ESI mass spectrum data: *m*/*z* 432.6187 ([M/2 − Cl]$^+$). ^{1}H NMR (600 MHz, DMSO-d_6): δ 2.33 (s, 6H), 5.93−5.94 (d, 2H, *J* = 8.9 Hz), 6.26−6.27 (d, 2H, *J* = 8.8 Hz), 7.28−7.29 (d, 1H, *J* = 8.9 Hz), 7.40−7.43 (t, 1H, *J* = 7.8 Hz), 7.51−7.53 (t, 1H, *J* = 6.6 Hz), 7.68−7.70 (d, 1H, *J* = 6.5 Hz), 7.73−7.75 (t, 1H, *J* = 7.5 Hz), 7.78−7.81 (m, 3H), 7.98−7.99 (t, 1H, *J* = 5.0 Hz), 8.07−8.10 (d-d, 1H, *J* = 5.4 Hz, *J* = 8.1 Hz), 8.19−8.27 (m, 4H), 8.35−8.36 (d, 1H, *J* = 5.0 Hz), 8.46−8.47 (m, 2H), 8.61−8.62 (d, 1H, *J* = 8.4 Hz), 8.65−8.66 (d, 1H, *J* = 5.4 Hz), 8.86−8.88 (d, 1H, *J* = 8.4 Hz), 8.94−8.95 (d, 1H, *J* = 8.2 Hz), 9.02−9.04 (d, 1H, *J* = 8.2 Hz), 9.21 (s, 1H), 9.24 (s, 1H), 9.36−9.37 (d, 1H, *J* = 8.0 Hz), 9.64−9.65 (d, 1H, *J* = 8.0 Hz), 9.70 (s, 1H). ^{13}C NMR (150 MHz, DMSO-d_6): δ 63.28, 111.46, 122.37, 124.18, 125.10, 125.40, 125.58, 128.44, 128.53, 128.59, 128.74, 129.15, 129.89, 130.05, 130.44, 132.33, 133.73, 134.15, 135.15, 135.17, 138.24, 138.31, 138.33, 138.73, 139.18, 139.56, 140.83, 141.01, 149.87, 149.96, 151.21, 151.32, 152.55, 152.81, 154.11, 156.00, 156.81, 157.05, 159.68, 169.52.

DFT Calculations. All calculations were performed using the Gaussian 09 suite of programs.[58] Full geometry optimizations were

https://dx.doi.org/10.1021/acs.inorgchem.0c01860
Inorg. Chem. XXXX, XXX, XXX−XXX

carried out for complexes **1**−**7** and $[Ru(bpy)_3]Cl_2$ by using the B3LYP density functional with the LanL2DZ basis set and an effective core functional used for the ruthenium atom, while the 6-31G(d,p) basis set was used for the other atoms.[59,60] The time-dependent density functional theory (TD-DFT) calculations were performed at the same level to predict the singlet electronic transitions and the UV−visible spectra.

$^1O_2$ Generation. The $^1O_2$ generation of complexes **1**−**7** was evaluated through monitoring the absorption spectral change at 378 nm of ABDA, and $[Ru(bpy)_3]Cl_2$ (Φ_Δ = 0.41 in water) was used as a standard in water. The experiment was conducted for complexes **1**−**7** (10 μM) in DMSO/water (1/99, v/v) containing ABDA (50 μM). The absorption spectra were recorded every 30 s under 465 ± 10 nm LED irradiation (1.26 J cm^{-2}) or every 4 min with red-light irradiation (650 ± 10 nm, xenon lamp with a band-pass filter, 19.2 J cm^{-2}). The Φ_Δ values were calculated with the equation $\Phi_\Delta(PS) = \Phi_\Delta(Std)S_{PS} \times F_{Std}/(S_{std} \times F_{PS})$, where PS designates the complexes **1**−**7** and Std designates $[Ru(bpy)_3]Cl_2$; S is the decomposition rate of ABDA at 378 nm, and F is the correction factor of absorption, which is given by $F = 1 - 10^{-OD}$ (OD denotes the optical density of complexes **1**−**7** and $[Ru(bpy)_3]Cl_2$ at 465 nm).

Cytotoxicity Assay of PDT. The photocytotoxicity of complexes **1**−**7** and $[Ru(bpy)_3]Cl_2$ against A549 and HepG2 cells was determined by means of an MTT (3-(4,5-dimethylthiazol-2-yl)-2,5-diphenyltetrazolium bromide) assay. Cells (10^4 per well) were seeded in 96-well plates and allowed to adhere for 24 h. After that, complexes **1**−**7** and $[Ru(bpy)_3]Cl_2$ were dissolved with DMF and diluted with the medium to the required concentrations (the final concentration of DMF was less than 0.4%). After being incubated in the dark for 4 h, cells were irradiated with 465 ± 10 nm nm LED irradiation (25.2 J cm^{-2}) or red light (650 ± 10 nm, 144.0 J cm^{-2}), and then the cells were incubated in the dark for a further 48 h. After that, the cells were stained with MTT (5 mg/mL) for another 5 h. The inhibition of cell growth was detected using an enzyme-labeling instrument. The IC_{50} values were calculated by SPSS software.

Cellular Accumulation. A549 cells with good viability were transferred into 6-well plates and cultured overnight at 37 °C. Then, complexes **4**, **7**, and $[Ru(bpy)_3]Cl_2$ were added with a concentration of 20 μM and incubated with the cells for 12 h. Then the supernatants were removed, and the cells were washed three times with ice-cold PBS. The cells were then digested with HNO_3 (65%), and the Ru contents were measured by ICP-MS.

Calcein AM and Propidium Iodide (PI) Costaining. For the calcein AM and propidium iodide (PI) costaining assay, A549 cells (10^5 per well) were seeded and cultured in confocal dishes overnight at 37 °C. Then complexes **4**, **7**, and $[Ru(bpy)_3]Cl_2$ were added to the cells with a final concentration of 1 μM. After 4 h of incubation, the cells were exposed to LED light (465 ± 10 nm, 25.2 J cm^{-2}) or red light (650 ± 10 nm, 144.0 J cm^{-2}). Thereafter, the cells were stained with Calcein AM/PI Double Stain Kit according to the instruction manual. Fluorescence images of the stained cells were then taken using a confocal microscope.

Intracellular ROS Production. The ROS generation in A549 cells was measured by DCFH-DA staining. A549 cells were seeded in a 6-well plate at a density of 2×10^5 cells/well and cultured for 12 h at 37 °C. Then, the tested complexes were added with a final concentration of 30 μM. After 4 h of incubation, DCFH-DA was added and the cells were incubated for another 30 min. Thereafter, the cells were washed with fresh medium three times followed by irradiation with 465 ± 10 nm LED light (25.2 J cm^{-2}) or red light (650 ± 10 nm, 144.0 J cm^{-2}). The photos were captured using a confocal microscope.

Gel Electrophoresis Study. DNA photocleavage activities of complexes **4**, **7**, and $[Ru(bpy)_3]Cl_2$ were evaluated by agarose gel electrophoresis. The tested complexes were first dissolved in DMF (10 mM) and then diluted to the desired concentrations with Tris-H_3PO_4 (50 mM, pH 7.2) buffer. The tested complexes (5 μL; lanes 1−9 0, 1, 5, 20, 40, 80, 160, 320, and 640 μM) and the final concentration of pBR322 plasmid DNA (50 ng/μL, 5 μL) were mixed together and irradiated with blue light (465 ± 10 nm, 12.5 J cm^{-2}) or red light (650 ± 10 nm, 72.0 J cm^{-2}). After 24 h of incubation, the mixtures (5 μL) with loading buffer (1 μL) were submitted to electrophoresis in agarose gel in TA buffer at 100 V for 90 min. Agarose gels were then dyed with ethidium bromide (0.5 mg/L) for 20 min. Bands were imaged by using a Molecular Imager (Bio-Rad, USA) under UV light.

Molecular Docking. A molecular docking simulation was carried out using AutoDock 4.2.[57] The crystal structure of the DNA duplex was obtained from the Protein Data Bank (PDB ID: 4JD8).[58] The docking procedure was conducted using a Lamarckian genetic algorithm for 200 docking runs. Visualization results were performed by PyMOL.

Apoptosis Analysis by Flow Cytometry. Complexes **4**, **7**, and $[Ru(bpy)_3]Cl_2$ with concentrations of IC_{50} values were added to the A549 cells. After incubation for 4 h, cells were irradiated with 465 ± 10 nm LED irradiation (25.2 J cm^{-2}) or red light (650 ± 10 nm, 144.0 J cm^{-2}). Then the cells were incubated in the dark for a further 24 h and collected by centrifugation (5 min, 25 °C, 2000 rpm). Afterward, the A549 cells were dyed by Annexin V-FITC/PI and analyzed with a flow cytometer.

■ ASSOCIATED CONTENT

Supporting Information

The Supporting Information is available free of charge at https://pubs.acs.org/doi/10.1021/acs.inorgchem.0c01860.

^1H and ^{13}C NMR and ESI mass spectra of complexes **1**−**7**, frontier molecular orbitals of complexes **1**−**7** and $[Ru(bpy)_3]Cl_2$, production of $^1O_2$ by complexes **1**−**7** and $[Ru(bpy)_3]Cl_2$ upon 650 nm irradiation and dose-dependent cell viability curves and synthetic route of **1**−**7**, confocal fluorescence images of calcein AM and propidium iodide (PI) costained A549 cells, cell accumulation of complexes **4**, **7**, and $[Ru(bpy)_3]Cl_2$ on A549 cells, and Cartesian coordinates of all optimized structures of complexes **1**−**7** and $[Ru(bpy)_3]^{2+}$ (PDF)

■ AUTHOR INFORMATION

Corresponding Authors

Jian Zhao − *Jiangsu Province Hi-Tech Key Laboratory for Biomedical Research and Pharmaceutical Research Center, School of Chemistry and Chemical Engineering, Southeast University, Nanjing 211189, People's Republic of China; Key Laboratory for Organic Electronics and Information Displays, Institute of Advanced Materials (IAM), Jiangsu National Synergetic Innovation Center for Advanced Materials (SICAM), Nanjing University of Posts and Telecommunications (NUPT), Nanjing 210023, People's Republic of China;* orcid.org/0000-0002-9365-7727; Email: zhaojianzhaokuan@163.com

Shaohua Gou − *Jiangsu Province Hi-Tech Key Laboratory for Biomedical Research and Pharmaceutical Research Center, School of Chemistry and Chemical Engineering, Southeast University, Nanjing 211189, People's Republic of China;* orcid.org/0000-0003-0284-5480; Email: sgou@seu.edu.cn

Qiang Zhao − *Key Laboratory for Organic Electronics and Information Displays, Institute of Advanced Materials (IAM), Jiangsu National Synergetic Innovation Center for Advanced Materials (SICAM), Nanjing University of Posts and Telecommunications (NUPT), Nanjing 210023, People's Republic of China;* orcid.org/0000-0002-3788-4757; Email: iamqzhao@njupt.edu.cn

Authors

Shuang Li − *Jiangsu Province Hi-Tech Key Laboratory for Biomedical Research and Pharmaceutical Research Center,*

https://dx.doi.org/10.1021/acs.inorgchem.0c01860
Inorg. Chem. XXXX, XXX, XXX−XXX

School of Chemistry and Chemical Engineering, Southeast University, Nanjing 211189, People's Republic of China

Xinyi Wang − *Jiangsu Province Hi-Tech Key Laboratory for Biomedical Research and Pharmaceutical Research Center, School of Chemistry and Chemical Engineering, Southeast University, Nanjing 211189, People's Republic of China*

Gang Xu − *Jiangsu Province Hi-Tech Key Laboratory for Biomedical Research and Pharmaceutical Research Center, School of Chemistry and Chemical Engineering, Southeast University, Nanjing 211189, People's Republic of China*

Complete contact information is available at: https://pubs.acs.org/10.1021/acs.inorgchem.0c01860

Notes

The authors declare no competing financial interest.

■ ACKNOWLEDGMENTS

We are grateful to the National Natural Science Foundation of China (Grants 21601034 and 21571033) and Jiangsu Province Natural Science Foundation (Grant BK20160664) for financial aid for this work. The Fundamental Research Funds for the Central Universities (Projects 2242019K40142) are also appreciated.

■ REFERENCES

(1) Zeng, L.; Gupta, P.; Chen, Y.; Wang, E.; Ji, L.; Chao, H.; Chen, Z.-S. The development of anticancer ruthenium(II) complexes: from single molecule compounds to nanomaterials. *Chem. Soc. Rev.* **2017**, *46*, 5771−5804.

(2) Liu, J.; Zhang, C.; Rees, T. W.; Ke, L.; Ji, L.; Chao, H. Harnessing ruthenium(II) as photodynamic agents: Encouraging advances in cancer therapy. *Coord. Chem. Rev.* **2018**, *363*, 17−28.

(3) Notaro, A.; Gasser, G. Monomeric and dimeric coordinatively saturated and substitutionally inert Ru(II) polypyridyl complexes as anticancer drug candidates. *Chem. Soc. Rev.* **2017**, *46*, 7317−7337.

(4) Poynton, F. E.; Bright, S. A.; Blasco, S.; Williams, D. C.; Kelly, J. M.; Gunnlaugsson, T. The development of ruthenium(II) polypyridyl complexes and conjugates for in vitro cellular and in vivo applications. *Chem. Soc. Rev.* **2017**, *46*, 7706−7756.

(5) Liu, J.; Lai, H.; Xiong, Z.; Chen, B.; Chen, T. Functionalization and cancer-targeting design of ruthenium complexes for precise cancer therapy. *Chem. Commun.* **2019**, *55*, 9904−9914.

(6) Farrer, N. J.; Salassa, L.; Sadler, P. J. Photoactivated chemotherapy (PACT): the potential of excited-state d-block metals in medicine. *Dalton. Trans.* **2009**, *0*, 10690−10701.

(7) Trondl, R.; Heffeter, P.; Kowol, C. R.; Jakupec, M. A.; Berger, W.; Keppler, B. K. NKP-1339, the first ruthenium-based anticancer drug on the edge to clinical application. *Chem. Sci.* **2014**, *5*, 2925−2932.

(8) Conti, L.; Bencini, A.; Ferrante, C.; Gellini, C.; Paoli, P.; Parri, M.; Pietraperzia, G.; Valtancoli, B.; Giorgi, C. Highly charged ruthenium(II) polypyridyl complexes as effective photosensitizer in photodynamic therapy. *Chem. - Eur. J.* **2019**, *25*, 10606−10615.

(9) Shum, J.; Leung, P. K. K.; Lo, K. K. W. Luminescent ruthenium(II) polypyridinecomplexes for a wide variety of biomolecular and cellular applications. *Inorg. Chem.* **2019**, *58*, 2231−2247.

(10) Li, A.; Turro, C.; Kodanko, J. J. Ru(II) polypyridyl complexes derived from tetradentate ancillary ligands for effective photocaging. *Acc. Chem. Res.* **2018**, *51*, 1415−1421.

(11) Lv, Z.; Wei, H.; Li, Q.; Su, X.; Liu, S.; Zhang, K. Y.; Lv, W.; Zhao, Q.; Li, X.; Huang, W. Achieving efficient photodynamic therapy under both normoxia and hypoxia using cyclometalated Ru(II) photosensitizer through type I photochemical process. *Chem. Sci.* **2018**, *9*, 502−512.

(12) Jakubaszek, M.; Goud, B.; Ferrari, S.; Gasser, G. Mechanisms of action of Ru(II) polypyridyl complexes in living cells upon light irradiation. *Chem. Commun.* **2018**, *54*, 13040−13059.

(13) Heinemann, F.; Karges, J.; Gasser, G. Critical overview of the use of Ru(II) polypyridyl complexes as photosensitizers in one-photon and two-photon photodynamic therapy. *Acc. Chem. Res.* **2017**, *50*, 2727−2736.

(14) Huang, H.; Yu, B.; Zhang, P.; Huang, J.; Chen, Y.; Gasser, G.; Ji, L.; Chao, H. Highly charged ruthenium(II) polypyridyl complexes as lysosome-localized photosensitizers for two-photon photodynamic therapy. *Angew. Chem., Int. Ed.* **2015**, *54*, 14049−14052.

(15) Zeng, L.; Kuang, S.; Li, G.; Jin, C.; Ji, L.; Chao, H. A GSH-activatable ruthenium(II)-azo photosensitizer for two-photon photodynamic therapy. *Chem. Commun.* **2017**, *53*, 1977−1980.

(16) Tian, N.; Sun, W.; Guo, X.; Lu, J.; Li, C.; Hou, Y.; Wang, X.; Zhou, Q. Mitochondria targeted and NADH triggered photodynamic activity of chloromethyl modified Ru(II) complexes under hypoxic conditions. *Chem. Commun.* **2019**, *55*, 2676−2679.

(17) Zheng, Y.; Zhang, D. Y.; Zhang, H.; Cao, J. J.; Tan, C. P.; Ji, L. N.; Mao, Z. W. Photodamaging of mitochondrial DNA to overcome cisplatin resistance by a Ru^{II}-Pt^{II} bimetallic complex. *Chem. - Eur. J.* **2018**, *24*, 18971−18980.

(18) He, L.; Liao, S. Y.; Tan, C. P.; Ye, R. R.; Xu, Y. W.; Zhao, M.; Ji, L. N.; Mao, Z. W. Ruthenium-arene-β-carboline complexes as potent inhibitors of cyclin-dependent kinase 1: synthesis, characterization and anticancer mechanism studies. *Chem. - Eur. J.* **2013**, *19*, 12152−12160.

(19) Ye, R. R.; Ke, Z. F.; Tan, C. P.; He, L.; Ji, L. N.; Mao, Z. W. Histone-deacetylase-targeted fluorescent ruthenium(II) polypyridyl complexes as potent anticancer agents. *Chem. - Eur. J.* **2013**, *19*, 10160−10169.

(20) Zamora, A.; Denning, C. A.; Heidary, D. K.; Wachter, E.; Nease, L. A.; Ruiz, J.; Glazer, E. C. Ruthenium-containing P450 inhibitors for dual enzyme inhibition and DNA damage. *Dalton. Trans.* **2017**, *46*, 2165−2173.

(21) Monro, S.; Colón, K. L.; Yin, H.; Roque, J., III; Konda, P.; Gujar, S.; Thummel, R. P.; Lilge, L.; Cameron, C. G.; McFarland, S. A. Transition metal complexes and photodynamic therapy from a tumor-centered approach: Challenges, opportunities, and highlights from the development of TLD1433. *Chem. Rev.* **2019**, *119*, 797−828.

(22) Wachter, E.; Heidary, D. K.; Howerton, B. S.; Parkin, S.; Glazer, E. C. Light-activated ruthenium complexes photobind DNA and are cytotoxic in the photodynamic therapy window. *Chem. Commun.* **2012**, *48*, 9649−9651.

(23) Jiang, J.; Qian, Y.; Xu, Z.; Lv, Z.; Tao, P.; Xie, M.; Liu, S.; Huang, W.; Zhao, Q. Enhancing singlet oxygen generation in semiconducting polymer nanoparticles through fluorescence resonance energy transfer for tumor treatment. *Chem. Sci.* **2019**, *10*, 5085−5094.

(24) Whittemore, T. J.; White, T. A.; Turro, C. New ligand design provides delocalization and promotes strong absorption throughout the visible region in a Ru(II) complex. *J. Am. Chem. Soc.* **2018**, *140*, 229−234.

(25) Sun, W.; Thiramanas, R.; Slep, L. D.; Zeng, X.; Mailander, V.; Wu, S. Photoactivation of anticancer Ru complexes in deep tissue: How deep can we go? *Chem. - Eur. J.* **2017**, *23*, 10832−10837.

(26) Foxon, S. P.; Alamiry, M. A.; Walker, M. G.; Meijer, A. J.; Sazanovich, I. V.; Weinstein, J. A.; Thomas, J. A. Photophysical properties and singlet oxygen production by ruthenium (II) complexes of benzo[i]dipyrido [3,2-a:2′,3-c] phenazine: spectroscopic and TD-DFT study. *J. Phys. Chem. A* **2009**, *113*, 12754−12762.

(27) Zhao, J.; Liu, N.; Sun, S.; Gou, S.; Wang, X.; Wang, Z.; Li, X.; Zhang, W. Light-activated ruthenium (II)-bicalutamide prodrugs for prostate cancer. *J. Inorg. Biochem.* **2019**, *196*, 110684.

(28) Sgambellone, M. A.; David, A.; Garner, R. N.; Dunbar, K. R.; Turro, C. Cellular toxicity induced by the photorelease of a caged bioactive molecule: design of a potential dual-action Ru (II) complex. *J. Am. Chem. Soc.* **2013**, *135*, 11274−11282.

(29) Zhang, Y.; Zhou, Q.; Tian, N.; Li, C.; Wang, X. Ru(II)-Complex-based DNA photocleaver having intense absorption in the phototherapeutic window. *Inorg. Chem.* **2017**, *56*, 1865−1873.
(30) Frei, A.; Rubbiani, R.; Tubafard, S.; Blacque, O.; Anstaett, P.; Felgenträger, A.; Maisch, T.; Spiccia, L.; Gasser, G. Synthesis, characterization, and biological evaluation of new Ru(II) polypyridyl photosensitizers for photodynamic therapy. *J. Med. Chem.* **2014**, *57*, 7280−7292.
(31) Karges, J.; Blacque, O.; Goldner, P.; Chao, H.; Gasser, G. Towards long wavelength absorbing photodynamic therapy photosensitizers via the extension of a $[Ru(bipy)_3]^{2+}$ core. *Eur. J. Inorg. Chem.* **2019**, *2019*, 3704−3712.
(32) Bahreman, A.; Cuello-Garibo, J. A.; Bonnet, S. Yellow-light sensitization of a ligand photosubstitution reaction in a ruthenium polypyridyl complex covalently bound to a rhodamine dye. *Dalton. Trans.* **2014**, *43*, 4494−4505.
(33) Zhou, Q. X.; Lei, W. H.; Li, C.; Hou, Y. J.; Wang, X. S.; Zhang, B. W. DNA photocleavage in anaerobic conditions by a Ru(II) polypyridyl complex with long wavelength MLCT absorption. *New J. Chem.* **2010**, *34*, 137−140.
(34) Zhou, Q. X.; Lei, W. H.; Chen, J. R.; Li, C.; Hou, Y. J.; Wang, X. S.; Zhang, B. W. A new heteroleptic ruthenium(II) polypyridyl complex with long-wavelength absorption and high singlet-oxygen quantum yield. *Chem. - Eur. J.* **2010**, *16*, 3157−3165.
(35) Mahmoud, W. H.; Mohamed, G. G.; El-Sayed, O. Y. Coordination compounds of some transition metal ions with new Schiff base ligand derived from dibenzoyl methane. Structural characterization, thermal behavior, molecular structure, antimicrobial, anticancer activity and molecular docking studies. *Appl. Organomet. Chem.* **2018**, *32*, No. e4051.
(36) El-Sonbati, A. Z.; Mahmoud, W. H.; Mohamed, G. G.; Diab, M. A.; Morgan, S. M.; Abbas, S. Y. Synthesis, characterization of Schiff base metal complexesand their biological investigation. *Appl. Organomet. Chem.* **2019**, *32*, No. e5048.
(37) Zhao, J.; Li, S.; Wang, X.; Xu, G.; Gou, S. Dinuclear organoruthenium complexes exhibiting antiproliferative activity through DNA damage and a reactive-oxygen-species-mediated endoplasmic reticulum stress pathway. *Inorg. Chem.* **2019**, *58*, 2208−2217.
(38) Hotze, A. C.; Faiz, J. A.; Mourtzis, N.; Pascu, G. I.; Webber, P. R.; Clarkson, G. J.; Yannakopoulou, K.; Pikramenou, Z.; Hannon, M. J. Far-red luminescent ruthenium pyridylimine complexes; building blocks for multinuclear arrays. *Dalton. Trans.* **2006**, *24*, 3025−3034.
(39) Bozic-Weber, B.; Constable, E. C.; Housecroft, C. E.; Neuburger, M.; Price, J. R. Sticky complexes: Carboxylic acid-functionalized N-phenylpyridin-2-ylmethanimine ligands as anchoring domains for copper and ruthenium dye-sensitized solar cells. *Dalton. Trans.* **2010**, *39*, 3585−3594.
(40) Juris, A.; Balzani, V.; Barigelletti, F.; Campagna, S.; Belser, P. L.; von Zelewsky, A. V. Ru (II) polypyridine complexes: photophysics, photochemistry, eletrochemistry, and chemiluminescence. *Coord. Chem. Rev.* **1988**, *84*, 85−277 1998.
(41) Higgins, S. L.; Brewer, K. J. Designing red-light-activated multifunctional agents for the photodynamic therapy. *Angew. Chem., Int. Ed.* **2012**, *51*, 11420−1422.
(42) Karges, J.; Heinemann, F.; Jakubaszek, M.; Maschietto, F.; Subecz, C.; Dotou, M.; Vinck, R.; Blacque, O.; Tharaud, M.; Goud, B.; Vinuelas Zahınos, E.; Spingler, B.; Ciofini, I.; Gasser, G. Rationally Designed Long-Wavelength Absorbing Ru(II) Polypyridyl Complexes as Photosensitizers for Photodynamic Therapy. *J. Am. Chem. Soc.* **2020**, *142*, 6578−6587.
(43) Lincoln, R.; Kohler, L.; Monro, S.; Yin, H.; Stephenson, M.; Zong, R.; Chouai, A.; Dorsey, C.; Hennigar, R.; Thummel, R. P.; McFarland, S. A. Exploitation of long-lived ^{3}IL excited states for metal-organic photodynamic therapy: verification in a metastatic melanoma model. *J. Am. Chem. Soc.* **2013**, *135*, 17161−17175.
(44) Reichardt, C.; Monro, S.; Sobotta, F. H.; Colón, K. L.; Sainuddin, T.; Stephenson, M.; Sampson, E.; John Roque, J., III; Yin, H.; Brendel, J. C.; Cameron, C. G.; McFarland, S.; Dietzek, B. Predictive strength of photophysical measurements for in vitro photobiological activity in a Series of Ru(II) polypyridyl complexes derived from π-extended ligands. *Inorg. Chem.* **2019**, *58*, 3156−3166.
(45) Sainuddin, T.; McCain, J.; Pinto, M.; Yin, H.; Gibson, J.; Hetu, M.; McFarland, S. A. Organometallic Ru(II) photosensitizers derived from π-expansive cyclometalating ligands: surprising theranostic PDT effects. *Inorg. Chem.* **2016**, *55*, 83−95.
(46) Yin, H.; Stephenson, M.; Gibson, J.; Sampson, E.; Shi, G.; Sainuddin, T.; Monro, S.; McFarland, S. A. In vitro multiwavelength PDT with ^{3}IL states: Teaching old molecules new tricks. *Inorg. Chem.* **2014**, *53*, 4548−4559.
(47) Rohrabaugh, T. N.; Collins, K. A.; Xue, C.; White, J. K.; Kodanko, J. J.; Turro, C. New Ru(II) complex for dual photochemotherapy: release of cathepsin K inhibitor and $^1O_2$ production. *Dalton. Trans.* **2018**, *47*, 11851−11858.
(48) Sun, Y.; Joyce, L. E.; Dickson, N. M.; Turro, C. Efficient DNA photocleavage by $[Ru(bpy)_2(dppn)]^{2+}$ with visible light. *Chem. Commun.* **2010**, *46*, 2426−2428.
(49) Zhao, J.; Zhang, X.; Fang, L.; Gao, C.; Xu, C.; Gou, S. Iridium(III) Complex-Derived Polymeric Micelles with Low Dark Toxicity and Strong NIR Excitation for Phototherapy and Chemotherapy. *Small* **2020**, *16*, 2000363.
(50) Albani, B. A.; Peña, B.; Leed, N. A.; De Paula, N. A.; Pavani, C.; Baptista, M. S.; Dunbar, K. R.; Turro, C. Marked improvement in photoinduced cell death by a new tris-heteroleptic complex with dual action: singlet oxygen sensitization and ligand dissociation. *J. Am. Chem. Soc.* **2014**, *136*, 17095−17101.
(51) Feng, Z.; Tao, P.; Zou, L.; Gao, P.; Liu, Y.; Liu, X.; Wang, H.; Liu, S.; Dong, Q.; Li, J.; Xu, B.; Huang, W.; Wong, W. Y.; Zhao, Q. Hyperbranched phosphorescent conjugated polymer dots with iridium(III) complex as the core for hypoxia imaging and photodynamic therapy. *ACS Appl. Mater. Interfaces* **2017**, *9*, 28319−28330.
(52) Nomula, R.; Wu, X.; Zhao, J.; Munirathnam, N. R. Photodynamic effect of light-harvesting, long-lived triplet excited state Ruthenium (II)-polyimine-coumarin complexes: DNA binding, photocleavage and anticancer studies. *Mater. Sci. Eng., C* **2017**, *79*, 710−719.
(53) Hartshorn, R. M.; Barton, J. K. Novel dipyridophenazine complexes of ruthenium(II): exploring luminescent reporters of DNA. *J. Am. Chem. Soc.* **1992**, *114*, 5919−5925.
(54) Sun, Y.; Joyce, L. E.; Dickson, N. M.; Turro, C. DNA photocleavage by an osmium (II) complex in the PDT window. *Chem. Commun.* **2010**, *46*, 6759−6761.
(55) Chen, X.; Gao, F.; Yang, W. Y.; Zhou, Z. X.; Lin, J. Q.; Ji, L. N. Structure activity relationship of polypyridyl ruthenium(II) complexes as DNA intercalators, DNA photocleavage reagents, and DNA topoisomerase and RNA polymerase inhibitors. *Chem. Biodiversity* **2013**, *10*, 367−384.
(56) Hall, J. P.; Cook, D.; Morte, S. R.; McIntyre, P.; Buchner, K.; Beer, H.; Cardin, D. J.; Brazier, J. A.; Winter, G.; Kelly, J. M.; Cardin, C. J. X-ray crystal structure of rac-$[Ru(phen)_2\ dppz]^{2+}$ with $d(ATGCAT)_2$ shows enantiomer orientations and water ordering. *J. Am. Chem. Soc.* **2013**, *135*, 12652−12659.
(57) Morris, G. M.; Huey, R.; Lindstrom, W.; Sanner, M. F.; Belew, R. K.; Goodsell, D. S.; Olson, A. J. AutoDock4 and AutoDockTools4: Automated docking with selective receptor flexibility. *J. Comput. Chem.* **2009**, *30*, 2785−2791.
(58) Frisch, M. J.; Trucks, G. W.; Schlegel, H. B.; Scuseria, G. E.; Robb, M. A.; Cheeseman, J. R.; Scalmani, G.; Barone, V.; Mennucci, B.; Petersson, G. A.; Nakatsuji, H.; Caricato, M.; Li, X.; Hratchian, H. P.; Izmaylov, A. F.; Bloino, J.; Zheng, G.; Sonnenberg, J. L.; Hada, M.; Ehara, M.; Toyota, K.; Fukuda, R.; Hasegawa, J.; Ishida, M.; Nakajima, T.; Honda, Y.; Kitao, O.; Nakai, H.; Vreven, T., Montgomery, J. A., Jr.; Peralta, J. E.; Ogliaro, F.; Bearpark, M. J.; Heyd, J.; Brothers, E. N.; Kudin, K. N.; Staroverov, V. N.; Kobayashi, R.; Normand, J.; Raghavachari, K.; Rendell, A. P.; Burant, J. C.; Iyengar, S. S.; Tomasi, J.; Cossi, M.; Rega, N.; Millam, N. J.; Klene, M.; Knox, J. E.; Cross, J. B.; Bakken, V.; Adamo, C.; Jaramillo, J.; Gomperts, R.; Stratmann, R. E.; Yazyev, O.; Austin, A. J.; Cammi, R.;

https://dx.doi.org/10.1021/acs.inorgchem.0c01860
Inorg. Chem. XXXX, XXX, XXX−XXX

Pomelli, C.; Ochterski, J. W.; Martin, R. L.; Morokuma, K.; Zakrzewski, V. G.; Voth, G. A.; Salvador, P.; Dannenberg, J. J.; Dapprich, S.; Daniels, A. D.; Farkas, O.; Foresman, J. B.; Ortiz, J. V.; Cioslowski, J.; Fox, D. J. *Gaussian 09, E01*; Gaussian, Inc.: Wallingford, CT, 2009.

(59) Wadt, W. R.; Hay, P. J. Ab initio effective core potentials for molecular calculations. Potentials for the transition metal atoms Sc to Hg. *J. Chem. Phys.* **1985**, *82*, 284−298.

(60) Becke, A. D. Density-functional exchange-energy approximation with correct asymptotic behavior. *Phys. Rev. A: At., Mol., Opt. Phys.* **1988**, *38*, 3098−3100.

https://dx.doi.org/10.1021/acs.inorgchem.0c01860
Inorg. Chem. XXXX, XXX, XXX−XXX